Journal of The Electrochemical Society

LiF as an Alloy Component or Slurry Additive in Si-Alloy Anodes

Journal of The Electrochemical Society, 2020 **167** 160524

LiF as an Alloy Component or Slurry Additive in Si-Alloy Anodes

R. S. Young,[1,2,*] B. Scott,[2] Congxiao Wei,[2] and M. N. Obrovac[1,2,,z]**

[1]*Department of Physics and Atmospheric Science, Dalhousie University, Halifax, N. S., B3H 4R2, Canada*
[2]*Department of Chemistry, Dalhousie University, Halifax, N. S., B3H 4R2, Canada*

Electrolyte additives are commonly used to improve electrochemical performance in Li-ion cells. The use of solids as electrolyte additives is far less common. Here, $Si_{40'}(FeSi_2)_{(60-x)'}(LiF)_{(x)'}$ ($' =$ volume percent) alloys with LiF incorporated in the alloy as a solid electrolyte additive are studied. Improved capacity retention was observed for LiF-containing alloys with $x < 12$, with optimum performance at $x = 6$. Improvements in electrochemical performance of Si-Fe alloys were also observed when LiF was introduced as a slurry additive. The use of solids as electrolyte additives may be a valuable method for improving electrochemical performance of Si-alloy negative electrodes.

 [DOI: 10.1149/1945-7111/abcf56]

Manuscript submitted July 16, 2020; revised manuscript received November 13, 2020. Published December 10, 2020.

Silicon-based negative electrode materials have been heavily researched as a means of increasing energy density in next-generation LIBs. By using Si based negative electrode materials, it is estimated that full cell energy density can be increased by as much as 34%.[1] Si is able to store 22.5 times more lithium per host atom than graphite which is conventionally used as a negative electrode material in LIBs, and, as a result Si, has a theoretical volumetric capacity of 2194 Ah l^{-1}, 3 times larger than that of graphite (719 Ah l^{-1}).[1] However, the electrochemical lithiation of Si causes a volume expansion as large as 280%, resulting in poor charge/discharge cycling characteristics.[1,2]

In order to decrease volume expansion and improve cycling performance, Si can be alloyed with an electrochemically inactive component such as iron.[1–3] It has additionally been shown that the addition of an inactive phase can decrease the potential at which $Li_{15}Si_4$ forms. $Li_{15}Si_4$ contributes directly to poor cycling performance as a result of the high stress generated at the two-phase reaction front during delithiation, causing particles to fracture and become mechanically disconnected.[4,5] In pure Si, $Li_{15}Si_4$ crystallizes at 50 mV.[4,5] By incorporating an inactive phase, $Li_{15}Si_4$ formation can be suppressed completely.[3,5]

LiF has been previously studied as a surface modifier to improve cycling performance of negative electrode materials. Wu et al. used LiF as a surface modifier for graphene, resulting in increased cycle life, and rate capability.[6] It was found that the LiF provided an extra Li source, lowering the initial irreversible capacity, while reducing SEI thickness, suppressing electrolyte side reactions, and enabling faster Li-ion transport.[6] Using density functional theory, Y. X. Lin et al. were able to show that a layer of LiF as thin as 2 nm can prevent electron tunneling from a lithium electrode, whereas Li_2CO_3, another well-known SEI component, requires 3 nm.[7] As a consequence, an effective SEI comprising LiF is formed thinner, resulting in the observed faster Li-transport. Fluorinated electrolyte additives are commonly used to form a thinner more stable SEI layer comprising LiF.[8–10] However, the use of fluorinated electrolyte additives can increase electrolyte cost and introduce irreversible capacity losses.

In this study, LiF is evaluated as a component in Si-Fe alloys. Being an inactive component, it is expected to improve cycling performance by reducing overall alloy volume expansion. LiF is slightly soluble in carbonate electrolytes (LiF solubility in dimethyl carbonate (DMC) is 1.07×10^{-5} mole fraction at 25 °C and 101.1 kPa).[11] Therefore, the presence of LiF in the alloy is additionally expected to act as an electrolyte additive, by keeping the electrolyte constantly saturated with LiF, so that it is continuously incorporated into the SEI.

Experimental

Si-$FeSi_2$-X (X = LiF) alloys were prepared from Si (99%, −325 mesh, Sigma-Aldrich), Fe (99.9%, −325 mesh, Sigma-Aldrich) and LiF (98.5%, −325 mesh, Alfa-Aesar) or Li_2CO_3 (99%, powder, Alfa-Aesar). A total of 0.5 ml of precursor powder was loaded into a 65 ml hardened steel milling vial (SPEX, model 8000-D, Spex CertiPrep, Metuchen, NJ) with 180 g of 1.6 mm stainless steel balls. Loaded vials were sealed under an argon atmosphere.[12] Initially alloys were prepared by loading all three components and ball milling simultaneously; however, it was found that the presence of LiF inhibited the mechanochemical reaction of Si and Fe. Instead, a two-step ball milling procedure was used where Si and Fe were first milled for 8 h, followed by the addition of LiF and an additional 8 h of milling.

SEM images were obtained with a TESCAN MIRA 3 field-emission SEM using a 5.0 kV accelerating potential. Both secondary electron (SE) and back-scattered electron (BSE) images were collected pre- and post-cycling. XRD patterns were collected using a Rigaku Ultima IV diffractometer with a Cu Kα X-ray source operating at 40 kV and 45 mA and a diffracted beam graphite monochromator.

Electrode slurries were prepared by mixing a 70:5:25 weight ratio of alloy:carbon black (Imerys Graphite and Carbon, Super C65): binder in an appropriate slurry solvent. For some electrodes the binder/slurry solvent was an aromatic polyimide (PI)/1-methyl-2-pyrrolidinone (NMP, 99.5%, Sigma-Aldrich) where the polyimide was added in the form of a 20% (w:w) solution of poly(amic acids) in NMP (Hitachi DuPont MicroSystems, LLC). For other electrodes the binder/slurry solvent was lithium polyacrylate (LiPAA)/water, where the LiPAA was added in the form of a polyacrylic acid solution (Sigma-Aldrich, average molecular weight 250,000 g $mole^{-1}$, 35 wt% in H_2O) neutralized with $LiOH{\cdot}H_2O$ (Sigma-Aldrich, 98%). Slurries were mixed using a high-shear mixer equipped with a Cowles blade for 10 min at a rotational frequency of 5000 rpm. Electrode slurries were coated onto electrolytic copper foil (Furukawa Electric, Japan) to a slurry thickness of 0.102 mm using a stainless-steel coating bar and dried at 120 °C for 1 h. 1.3 cm^2 electrode disks were cut from the coatings. Electrodes with PI binder were subsequently cured by heating at 300 °C for 4 h under flowing argon, as described in Ref. 13.

Electrodes were assembled into 2325-type coin cells with a lithium foil counter/reference electrode separated by one layer each of Celgard 2300 and blown polypropylene microfiber (BMF)

*Electrochemical Society Student Member.
**Electrochemical Society Member.
[z]E-mail: mnobrovac@dal.ca

separator (3 M Co.). The cells were assembled in an Ar-filled glove box using 100 μl of electrolyte. Electrolyte consisted of either 1 M $LiPF_6$ (BASF, 99.94%, water content 14 ppm) in (v:v) (3:6:1) ethylene carbonate (EC):diethyl carbonate (DEC) (BASF, 98%, water content < 50 ppm):fluoroethylene carbonate (FEC) (BASF, >99.94%) or 1 M $LiPF_6$ in (v:v) EC:DEC (1:2).

Cells were cycled at 30.0 ± 0.1 °C between 0.005 V and 0.9 V with a Maccor Series 4000 Automated Test System at a rate of C/10 for the first cycle and C/5 for subsequent cycles. To simulate CCCV full cell charging, cells were held at 5 mV at the end of each cycle until a C/20 current limit was reached. C-rates were determined based on a theoretical 3578 mAh g^{-1} active Si capacity. The fade rate was defined as the average percent capacity fade per cycle encountered between cycles 10 and 80.

Symmetric cells were assembled in 2325-type coin cells with two identical electrodes separated by two layers of Celgard 2300 and one layer of blown polypropylene microfiber (BMF). One of the electrodes is prepared in a lithiated state, while the other is in a delithiated state, as follows. The delithiated electrode was lithiated to a potential of 0.005 V and then delithiated to 0.9 V at a rate of C/20. The lithiated electrode was lithiated to a potential of 0.005 V, delithiated to 0.9 V at a rate of C/20 and then lithiated to 0.005 V at a C/5 rate and held at this potential until the current dropped below C/20.

Electrochemical impedance spectroscopy (EIS) was performed with a Biologic VMP-3 potentiostat where alternating current (AC) impedance spectra were collected with 10 points per decade from 100 kHz to 10 mHz with a 10 mV amplitude signal. In this work total impedance values, (R_{tot}), represent the diameter of the semicircle in the Nyquist plot, which corresponds to the sum of the charge transfer resistance and the resistance of lithium ions transporting through the SEI layer.[14]

Results and Discussion

A series of ball milled Si-Fe-LiF alloys were prepared such that their volume expansion upon full lithiation was always 112%. This corresponds to an active Si volume fraction of 40%.[2] This composition range is shown in Figs. 1a and 1b in terms of volume percent and mole percent of each component, respectively. This series can be represented in terms of volume percent as $Si_{40'}(FeSi_2)_{(60-x)'}(LiF)_{(x)'}$ where the primed quantities are used to indicate volume percents, in order to differentiate them from conventional chemical formula units. XRD patterns of ball milled $Si_{40'}(FeSi_2)_{(60-x)'}(LiF)_{(x)'}$ (x = 0 and x = 30) alloys are shown in Fig. 2a. When there is no LiF present, crystalline Si (cr-Si) and Fe react, forming $FeSi_2$ and amorphous-Si (a-Si). However, when LiF is present, a peak corresponding to unmilled cr-Si is present in the XRD pattern. Apparently, the presence of LiF impedes the amorphization of Si during ball milling. In order to obtain an amorphous active Si phase for each sample, milling was conducted in two steps. In the first step only Si and Fe were milled, to form a Si-Fe alloy with a completely amorphous active Si phase. This was followed by a second milling step to incorporate LiF. XRD patterns of alloys synthesized using this two-step method are shown in Fig. 2b. These alloys consist of a-Si, LiF and $FeSi_2$. As the LiF content is increased there is a proportional increase in the intensity of the LiF peaks in the XRD patterns and a simultaneous decrease in the $FeSi_2$ peak intensity, as expected.

Symmetric cells were constructed in order to determine the effect of LiF additions in $Si_{40'}(FeSi_2)_{(60-x)'}(LiF)_{(x)'}$ on impedance. Electrochemical impedance spectra of $Si_{40}(FeSi_2)_{(60-x)}(LiF)_{(x)}$ (x = 0 and 12) electrodes measured prior to cycling and after 10, 20, and 30 cycles are shown in Fig. 3a and the corresponding R_{tot} values are shown in Fig. 3b. Electrodes containing LiF had higher impedance initially. This is expected, since LiF is both an electronic and ionic insulator. During initial cycling, the impedance of both electrodes decreased. This has been observed previously by Yan et al. and may be due to a decrease in electronic resistance as the electrode expands and the alloy particles become more tightly packed.[15] However, R_{tot} decreases more rapidly during initial cycles, to nearly match that of the pure Si-Fe alloy after 10 cycles, possibly because of more efficient SEI formation and reduced alloy degradation, as will be shown below.

Potential profiles and differential capacity plots of $Si_{40'}(FeSi_2)_{(60-x)'}(LiF)_{(x)'}$ electrodes cycled in half-cells are shown in Figs. 4a and 4b. The potential profiles and differential capacity curves are characteristic of a-Si with two sloping plateaus and no evidence of $Li_{15}Si_4$ formation. All of the potential profiles are similar for $x \leqslant 12$. larger LiF content results in decreased initial coulombic efficiency (ICE), lower reversible capacity, and fade. We speculate that this may be due to the partial solubility of LiF in the electrolyte, which may lead to alloy degradation for high LiF contents.

Figure 5a shows the cycling performance of the $Si_{40'}(FeSi_2)_{(60-x)'}(LiF)_{(x)'}$ electrodes. For small values of x, as the LiF content increases, the specific capacity also increases. This is expected since the molar mass of the electrode decreases as $FeSi_2$ (4.95 g ml^{-1}) is replaced by an equal volume of LiF (2.64 g ml^{-1}). To account for this change in molar mass, capacities were normalized according to their first delithiation capacity, as shown in Fig. 5b. The pure Si-Fe alloy (x = 0) has a capacity retention of nearly 80% after 80 cycles. The capacity retention increases significantly, to over 95%, as the LiF content is increased to x = 9. As LiF content is further increased there is a continual decrease in capacity. This is likely caused by the degradation of the $Si_{40'}(FeSi_2)_{(60-x)'}(LiF)_{(x)'}$ alloys with high LiF contents, due to LiF solubility, as mentioned above.

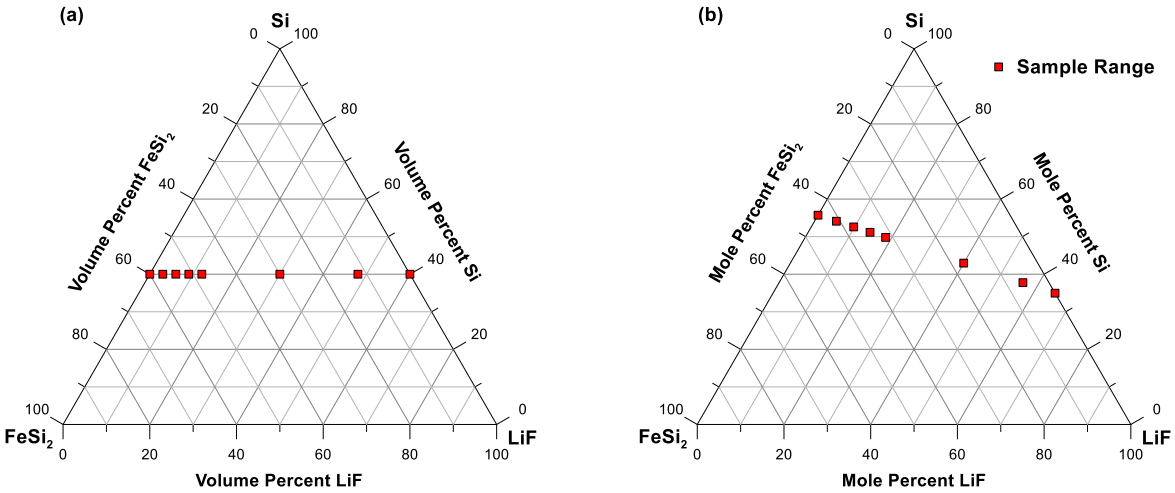

Figure 1. Ternary Si-$FeSi_2$-LiF composition diagrams in terms of (a) volume percent and (b) mole percent. The red squares indicate the compositions explored in this work.

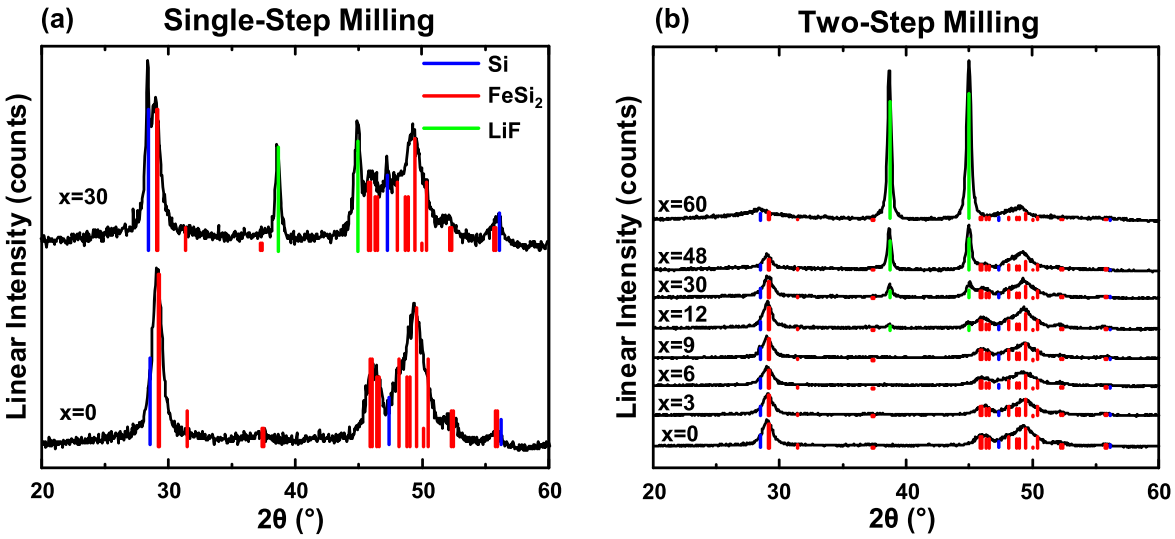

Figure 2. XRD patterns of $Si_{40'}(FeSi_2)_{(60-x)'}(LiF)_{(x)'}$ prepared by (a) milling in a single step, and (b) milling in two-steps.

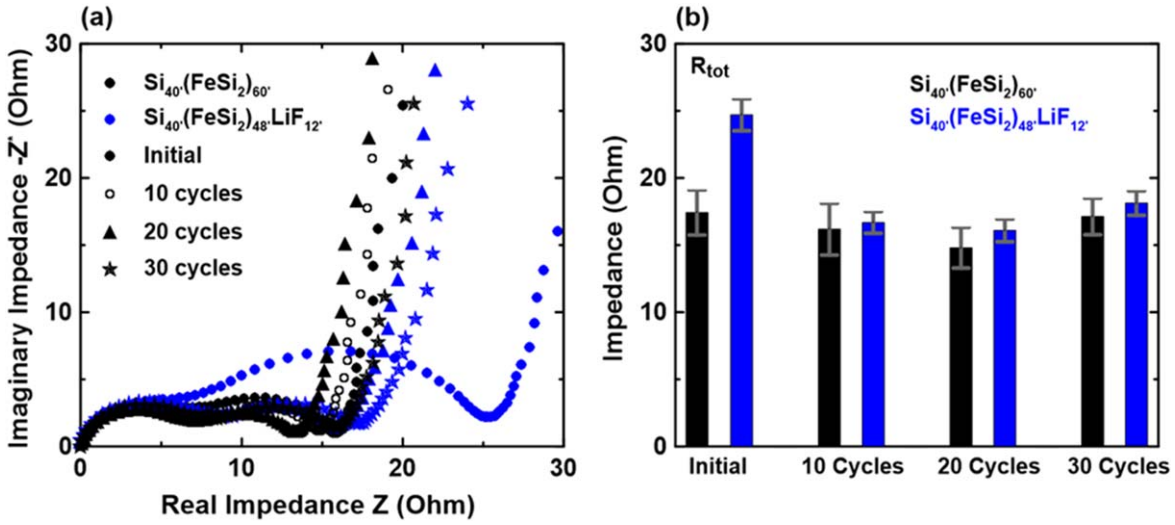

Figure 3. (a) Nyquist plots of $Si_{40'}(FeSi_2)_{(60-x)'}(LiF)_{(x)'}$ electrodes where x = 0 and 12, and (b) corresponding R_{tot} values. Error bars were calculated based on three duplicate cells for each experiment.

Figure 5c shows the coulombic efficiency (CE) of the $Si_{40'}(FeSi_2)_{(60-x)'}(LiF)_{(x)'}$ electrodes. The pure Si-Fe alloy has a steady-state CE of about 99.6%. A slightly improved CE of 99.8% is observed when x = 6. Poor CE is observed for higher values of x, as expected. In half-cell testing, capacity retention is thought to be related to electrode mechanical integrity, while CE is related to the extent of electrolyte reactions at the electrode surface. Indeed, this is the case as can be seen in Fig. 6, which shows cross-sectional BSE-SEM images of $Si_{40'}(FeSi_2)_{(60)'}$ and $Si_{40'}(FeSi_2)_{(54)'}(LiF)_{(6)'}$ electrodes before and after cycling. In Fig. 6a, both $Si_{40'}(FeSi_2)_{(60)'}$ and $Si_{40'}(FeSi_2)_{(54)'}(LiF)_{(6)'}$ alloy particles prior to cycling are appear bright in the images, due to the high contrast between the iron containing alloy and the polymer binder and carbon black between the alloy particles. In addition, the pristine alloy particles have sharp definite edges. After cycling, both electrodes show signs of fracture surface erosion, as has been observed previously for alloy particles,[16] however the extent of the degradation is much less in the $Si_{40'}(FeSi_2)_{(54)'}(LiF)_{(6)'}$ alloy. This can be seen more clearly in the lower magnification images shown in Fig. 6b. The difference is striking. Almost all of the $Si_{40'}(FeSi_2)_{(60)}$ alloy has been eroded after 100 cycles, whereas most of the $Si_{40'}(FeSi_2)_{(54)'}(LiF)_{(6)'}$ alloy still intact. The above results imply that small additions of LiF to alloys aid in maintaining alloy mechanical integrity and in reducing electrolyte reactivity. This may be accomplished via a thinner, more stable SEI formation with small additions of LiF. Figure 7 displays the results of cycling the $Si_{40'}(FeSi_2)_{(60-x)'}(LiF)_{(x)'}$ alloys in electrolyte with and without FEC additive. $Si_{40'}(FeSi_2)_{(60)'}$ alloy shows rapid capacity fade (~0% capacity retention/60cycles) when no FEC is present. Additions of LiF result in significant cycling improvement, with $Si_{40'}(FeSi_2)_{(54)'}(LiF)_{(6)'}$ having 60% capacity retention after 80 cycles. When FEC is added, the fade rate of the $Si_{40'}(FeSi_2)_{(60)'}$ alloy is lower (75% capacity retention/80 cycles) to what was achieved by adding LiF alone. However, the best capacity retention is obtained when both FEC and LiF are utilized (85% capacity retention/80 cycles). Therefore, LiF and FEC seem to be additive in their ability to improve capacity retention.

LiF was then used as a slurry additive to determine whether the addition of LiF to the alloy by ball milling was necessary. $Si_{40'}(FeSi_2)_{(60-x)'}$ alloys were prepared where x = 0, 6, and 9; and LiF component was incorporated as an additive in the electrode slurry, so that the final electrode composition was identical to the $Si_{40'}(FeSi_2)_{(60-x)'}(LiF)_{(x)'}$ series alloys. Electrochemical performance

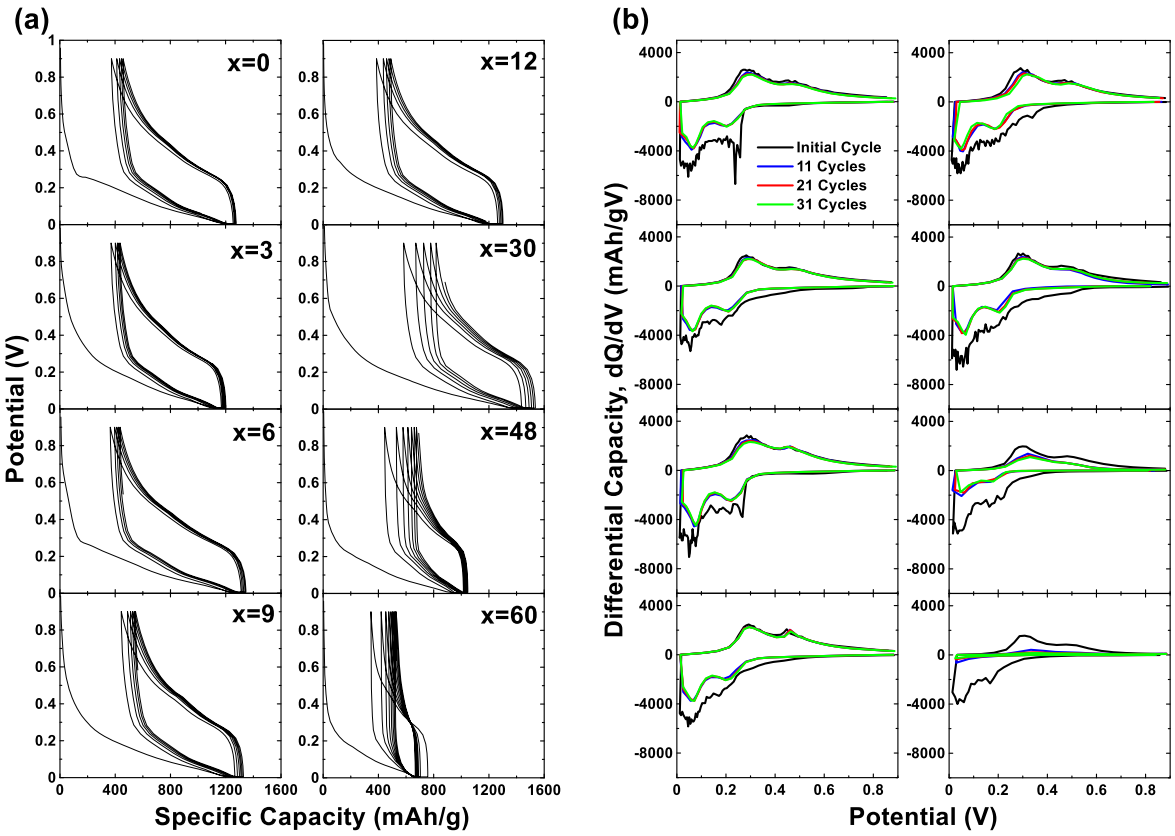

Figure 4. (a) Potential profiles and (b) differential capacity curves of $Si_{40}(FeSi_2)_{(60-x)}(LiF)_{(x)}$ electrodes.

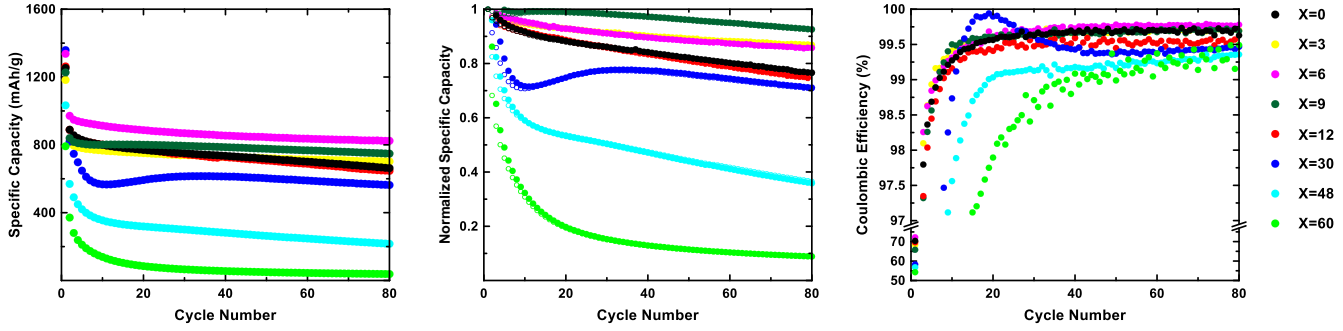

Figure 5. (a) Specific capacity vs cycle number, (b) normalized capacity vs cycle number, and c) columbic efficiency vs cycle number of $Si_{40}(FeSi_2)_{(60-x)}(LiF)_{(x)}$ electrodes.

was evaluated in FEC-containing and FEC-free electrolyte, shown in Fig. 8. When electrolyte contained FEC, improved capacity retention was observed for x = 6 and 9, compared to x = 0. The improvement for x = 9 was identical to when the LiF was incorporated directly in the alloy. However, for x = 6, the best performing formulation (13.00% fade rate) did not have the degree of improvement as when the LiF was incorporated directly in the alloy (9.78% fade rate). To test the effects of LiF grain size when used as a slurry additive, LiF (98.5%, −325 mesh, Alfa-Aesar) was ball milled for 8 h before being added into the slurry. No significant difference was observed. Therefore, the addition of LiF directly to electrode slurries can be a facile method for improving electrochemical performance of Si-alloy negative electrodes. However, in this instance incorporating LiF directly in the alloy is superior. When the electrolyte did not contain FEC, LiF additions to the slurry caused rapid capacity fade. This behavior is typical of rapid mechanical failure of the electrode. It is difficult to understand why this is not a failure mode when FEC is present. We suspect that when FEC is present, FEC decomposition products already saturate the electrolyte with LiF, limiting the dissolution of the LiF that is incorporated in the electrode, thereby reducing the electrode mechanical failure.

Conclusions

LiF was added as a solid electrolyte additive in the form of an inactive alloy component to Si-Fe alloys. It was found that in order to maintain a nanocrystalline microstructure, it was necessary to first ball mill the Si and Fe components of the alloy and then incorporate LiF in a second ball milling step. $Si_{40}(FeSi_2)_{(60-x)}(LiF)_{(x)}$ alloys showed improved electrochemical performance and capacity retention when x = 3, 6, and 9. It was also shown that when LiF was added as a slurry additive to electrodes containing Si-Fe alloys, improved cycling performance could also be achieved when FEC was also present in the electrolyte, however the improvement was not as great as when the LiF was incorporated directly into the Si-Fe alloy. The addition of electrode additives by ball milling or as a

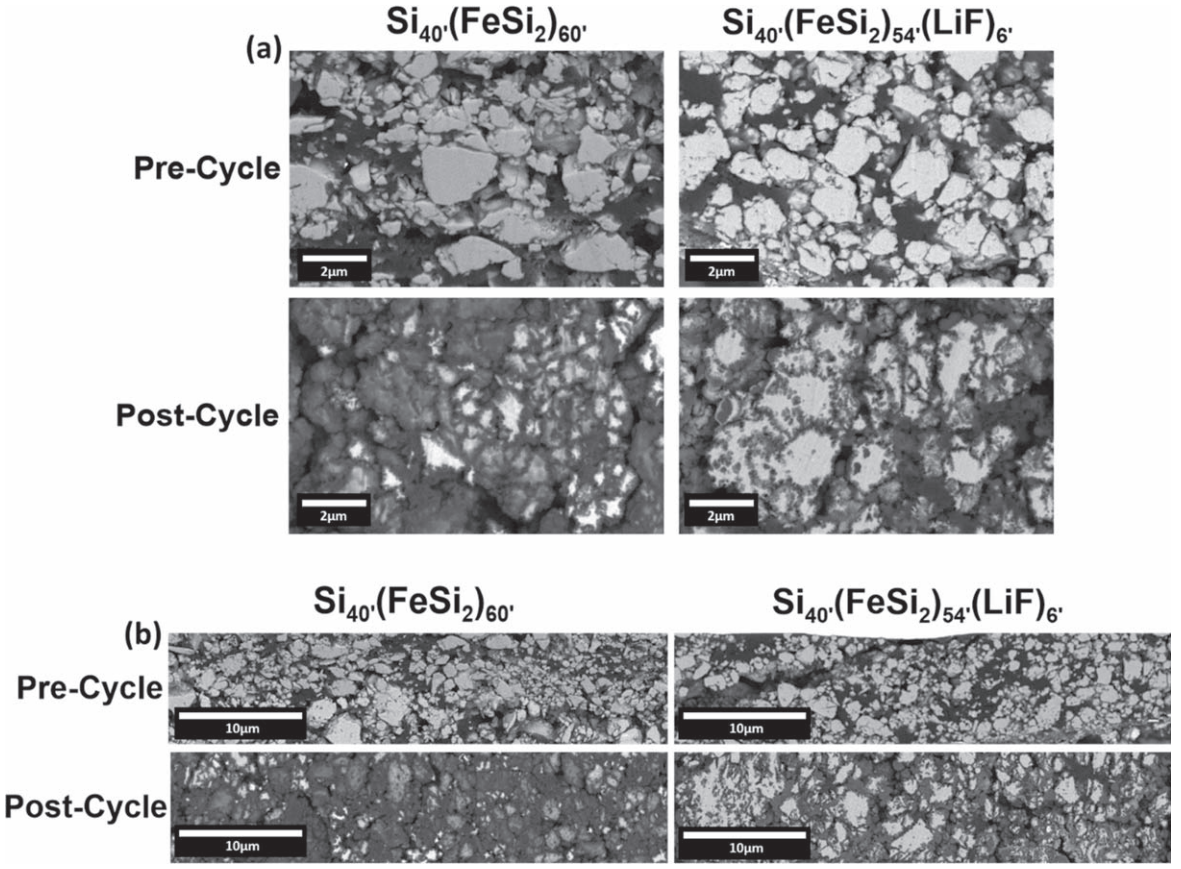

Figure 6. Cross-sectional BSE-SEM images of $Si_{40'}(FeSi_2)_{(60-x)'}(LiF)_{(x)'}$ for x = 0 and 6, pre and post cycling. (a) high magnification, (b) lower magnification.

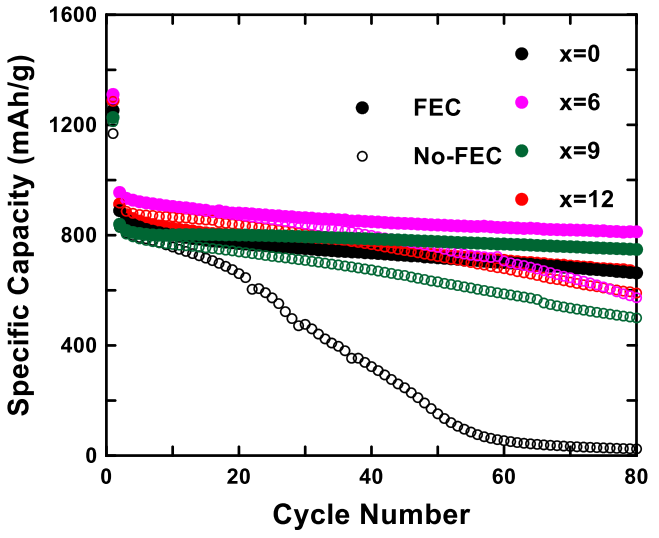

Figure 7. Cycling performance of $Si_{40'}(FeSi_2)_{(60-x)'}(LiF)_{(x)'}$ electrodes in FEC containing and FEC-free electrolyte.

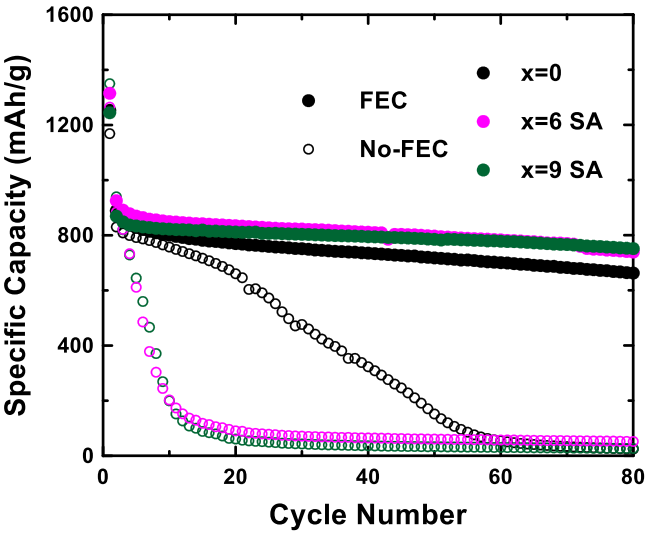

Figure 8. Cycling performance $Si_{40'}(FeSi_2)_{(60-x)'}$ where $(LiF)_{(x)'}$ was incorporated as a slurry additive (SA) using FEC containing and FEC-free electrolyte.

slurry additive may be valuable methods for improving electrochemical performance that can be used in conjunction with more traditional alloy compatible binders and liquid electrolyte additives.

Acknowledgments

The authors acknowledge financial support from NSERC, Novonix Battery Testing Services Inc., the Canada Foundation for Innovation, and the Atlantic Innovation Fund for this work.

ORCID

R. S. Young https://orcid.org/0000-0002-4478-7656
M. N. Obrovac https://orcid.org/0000-0001-5509-3185

References

1. M. N. Obrovac and V. L. Chevrier, *Chem. Rev.*, **114**, 11444 (2014), http://ncbi.nlm.nih.gov/pubmed/25399614.

2. M. N. Obrovac, L. Christensen, D. B. Le, and J. R. Dahn, *J. Electrochem. Soc.*, **154**, A849 (2007).
3. Z. Du, R. A. Dunlap, and M. N. Obrovac, *J. Electrochem. Soc.*, **163**, A2011 (2016).
4. M. N. Obrovac and L. Christensen, *Electrochem. Solid-State Lett.*, **7**, A93 (2004).
5. D. S. M. Iaboni and M. N. Obrovac, *J. Electrochem. Soc.*, **163**, A255 (2016).
6. Z. S. Wu et al., *Adv. Funct. Mater.*, **22**, 3290 (2012).
7. Y. X. Lin, Z. Liu, K. Leung, L.-Q. Chen, P. Lu, and Y. Qi, *J. Power Sources*, **309**, 221 (2016).
8. M. N. Obrovac, *Curr. Opin. Electrochem.*, **9**, 8 (2018).
9. L. Ma, L. Ellis, S. L. Glazier, X. Ma, and J. R. Dahn, *J. Electrochem. Soc.*, **165**, A1718 (2018).
10. A. Schiele et al., *ACS Energy Lett.*, **2**, 2228 (2017).
11. N. Xin, Y. Sun, M. He, C. Radke, and J. Prausnitz, *Fluid Phase Equilib.*, **461**, 1 (2017).
12. T. D. Hatchard, A. Genkin, and M. N. Obrovac, *AIP Adv.*, **7** (2017).
13. B. N. Wilkes, Z. L. Brown, L. J. Krause, M. Triemert, and M. N. Obrovac, *J. Electrochem. Soc.*, **163**, A364 (2016).
14. R. Petibon, L. Madec, D. W. Abarbanel, and J. R. Dahn, *J. Power Sources*, **300**, 419 (2015).
15. Z. Yan, C. Wei, and M. N. Obrovac, *J. Power Sources*, **438**, 1 (2019).
16. L. J. Krause, T. Brandt, V. L. Chevrier, and L. D. Jensen, *J. Electrochem. Soc.*, **164**, A2277 (2017).